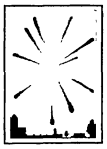

Meteoritics & Planetary Science 37, 835–854 (2002)
Available online at http://www.uark.edu/meteor

Sayh al Uhaymir 094: A new martian meteorite from the Oman desert

E. GNOS[1]*, B. HOFMANN[2], I. A. FRANCHI[3], A. AL-KATHIRI[4], M. HAUSER[1] AND L. MOSER[1]

[1]Institute for Geological Sciences, Baltzerstrasse 1, 3012 Berne, Switzerland
[2]Natural History Museum Bern, Bernastrasse 15, 3005 Berne, Switzerland
[3]Planetary Sciences Research Institute, Open University, Milton Keynes MK7 6AA, United Kingdom
[4]Directorate General of Minerals, Ministry of Commerce and Industry, Salalah, Sultanate of Oman
*Correspondence author's e-mail address: gnos@geo.unibe.ch

(Received 2001 November 7; accepted in revised form 2002 March 12)

Abstract–Sayh al Uhaymir (SaU) 094 is a 223.3 g, partially crusted, strongly to very strongly shocked melanocratic olivine-porphyric rock of the shergottite group showing a microgabbroic texture. The rock consists of pyroxene (52.0–58.2 vol%)—dominantly prismatic pigeonite ($En_{60-68}Fs_{20-27}Wo_{7-9}$) associated with minor augite ($En_{46-49}Fs_{15-16}Wo_{28-31}$)—brown (shock-oxidized) olivine (Fo_{65-69}; 22.1–31%), completely isotropic interstitial plagioclase glass (maskelynite; $An_{50-64}Or_{0.3-0.9}$; 8.6–13.0%), chromite and titanian magnesian chromite (0.9–1.0%), traces of ilmenite (Ilm_{80-86}), pyrrhotite (Fe_{92-100}; 0.1–0.2%), merrillite (<<0.1%), and pockets (4.8–6.7%) consisting of green basaltic to basaltic andesitic shock glass that is partially devitrified into a brown to black product along boundaries with the primary minerals. The average maximum dimensions of minerals are: olivine (1.5 mm), pyroxene (0.3 mm) and maskelynite (0.3 mm). Primary melt inclusions in olivine and chromite are common and account for 0.1–0.6% of the rock. X-ray tomography revealed that the specimen contains ~0.4 vol% of shock-melt associated vesicles, up to 3 mm in size, which show a preferred orientation. Fluidization of the maskelynite, melting and recrystallization of pyroxene, olivine and pyrrhotite indicate shock stage S6. Minor terrestrial weathering resulted in calcite-veining and minor oxidation of sulfides. The meteorite is interpreted as paired with SaU 005/008/051. The modal composition is similar to Dar al Gani 476/489/670/735/876, with the exception that neither mesostasis nor titanomagnetite nor apatite are present and that all phases show little zonation. The restricted mineral composition, predominance of chromite among the oxides, and abundance of olivine indicate affinities to the lherzolitic shergottites.

INTRODUCTION

Twenty-four unpaired meteorites presently known are attributed to Mars. The most compelling evidence that links them to Mars are relative abundances and isotopic compositions of trapped gases in shergottite shock glasses that are in agreement with direct martian atmosphere compositions measured by the 1976 Viking lander missions (*e.g.*, Bogard and Johnson, 1983). Most martian meteorites are differentiated rocks characterized by young crystallization ages, characteristic C, N, O and noble gas isotopic compositions (*e.g.*, Clayton and Mayeda, 1996; Dreibus and Wänke, 1987; Wänke, 1991), and distinct major and trace element concentrations (*e.g.*, Steele and Smith, 1982; McSween and Jarosewich, 1983; Lodders, 1998). To this suite belong basaltic, gabbroic and lherzolithic rocks (shergottites), clinopyroxenites-wehrlites (nakhlites), a dunite (Chassigny) and an orthopyroxenite. Since the report of putative biological signatures in the martian meteorite Allan Hills (ALH) 84001 (McKay *et al.*, 1996), and in context with intense exploration of Mars by space missions, publications on Mars meteorites have exploded. At the same time, the number of known independent Mars meteorites has increased from 12 to presently 24 (total weight of ~83 kg) since the recent compilations on martian meteorites by McSween and Treiman (1998) and Papike (1998). The new martian meteorite described here was found in the Sayh al Uhaymir region in interior Oman in February 2001 by two of us (M. H. and L. M.) in a joint meteorite search campaign with the Ministry of Commerce and Industry, Sultanate of Oman and was named Sayh al Uhaymir (SaU) 094 (Grossman and Zipfel, 2001). The rock was sampled on flat-bedded Miocene fresh-water limestone deposits of the Fars group (Le Métour *et al.*, 1995). The meteorite is very likely paired with SaU 005, 008 and 051 (Grossmann, 2000; Grossman and Zipfel, 2001) because all were found within a few kilometers distance and are macroscopically similar.

The aim of this paper is to report on the petrography, mineralogy and shock metamorphism of SaU 094. Chemical

Prelude preprint MS#4704

investigations and age dating (terrestrial age, exposure age, formation/ejection ages) are under way.

ANALYTICAL METHODS

Before cutting we applied x-ray tomography to the meteorite at the Federal Material Testing Laboratory (EMPA, Dübendorf) to non-destructively obtain information about its interior. The industrial computer tomography (CT) scanner applied was made by Scientific Measurement Systems (SMS, Austin, Texas). It was operated at 400 kV, 2.25 mA using linear array detectors, detector aperture 0.25 × 0.5 mm. Tomographs obtained had a resolution of 0.1 mm (pixel size).

Doubly polished thin sections were studied by transmitted and reflected light microscopy, carbon coated and then used for microprobe and cathode luminescence (25 kV, 80 nA) investigations. Because maskelynite and shock glass are isotropic and show little chemical variation we used standard oils and the immersion method for determination of refractive indices on small fragments of maskelynite and shock glass.

Mineral compositions were obtained on a Cameca SX-50 microprobe at Bern University using natural and synthetic mineral standards, wavelength dispersive spectrometers, and beam conditions of 15 kV and 20 nA for silicates, oxides, sulfides and glass. Sulfide standards were used for analyzing the sulfides. Counting times were 20 s on peak and background for major elements, and up to 60 s for trace elements. For all glasses the spot size was ~15 μm. The possibility of element diffusion during glass analysis was excluded by analyzing the same spot several times in sequence and using different measurement times, which resulted in no variation. For phosphate analysis we used rare earth element (REE) phosphate or REE glass standards, peak and background settings as described by Scherrer *et al.* (2000), a 10 μm spot and 25 kV, 20 nA beam conditions with 100 s REE counting times. Data were reduced using the PAP procedure.

Small vesicles and alteration products therein were examined using scanning electron microscopy of selected vesicle-rich rock chips. Samples were gold-coated.

Oxygen isotopic composition was determined by laser fluorination of powdered aliquots following the procedure described in Miller *et al.* (1999).

PETROGRAPHY AND MINERALOGY

Sayh al Uhaymir 094 is 4 × 7 × 5 cm in size, weighs 223.3 g and has a relatively angular shape. Two of the rock's four main faces are coated by very thin black fusion crust (rock color chart RCC 5YR 2/1), the other two are broken surfaces of brownish tint (10YR 4/1). Millimeter-sized dark olivine megacrysts are macroscopically visible on its surface and in cut sections (Fig. 1). On a cut surface, the olivine megacrysts appear brownish gray to black (RCC 5YR 3/1) and are set in an olive-gray (5Y 4/1) groundmass consisting of maskelynite and clinopyroxene (Fig. 1a,b,c). On the surface of the meteorite a few fractures, up to 4 cm in length, are apparent.

X-ray tomographs allowed us to distinguish areas rich in olivine (dark speckles), areas consisting of maskelynite and clinopyroxene (lighter gray speckles), and unexpectedly large, millimeter-sized vesicles present throughout the rock (Fig. 2). Most of these vesicles, which characteristically form the central part of larger shock melt pockets, seem unrelated to fractures.

The primary identification of the rock (Grossman and Zipfel, 2001) was made on five polished thin sections of <1 mm sized fragments from the surface of the meteorite. After cutting of the rock three additional thin sections were prepared perpendicular to one of the faces of the meteorite showing a fusion crust (Fig. 1b,c).

In thin section SaU 094 shows an olivine-porphyric texture without obvious foliation or lineation (Figs. 1 and 3a). Yellowish to dark brown (commonly patchy) hypidiomorphic olivine crystals or clusters of crystals (average maximum dimension 1.5 mm) are embedded in a fine-grained groundmass consisting of prismatic light cream-colored clinopyroxene crystals (mostly pigeonite) and interstitial feldspathic glass (maskelynite) (average maximum dimension 0.3 mm; Fig. 3a). Point counting of two thin sections yielded 22.1–31.0 vol% olivine, 52.0–58.2% pyroxene (pigeonite and augite were not distinguishable) and 8.6–13.0% maskelynite (Table 1). Accessory minerals are chromite (0.9–1.0%), pyrrhotite ± pentlandite (0.1–0.2%) and traces of merrillite. Melt inclusions in olivine (Fig. 3b), chromite and pyroxene account for 0.1–0.6%, and shock melts (Fig. 3c) for 4.8–6.7% of the rock. 4.0–4.1% of this shock melt is finely recrystallized and dark brown to black; the remaining 0.7–2.7% consists of fresh green glass (Table 1). Maskelynite displays a dark bluish-green cathode luminescence without obvious zonation. The fusion crust, though externally visible over significant portions of the meteorite's surface, was only occasionally encountered in thin section. In contrast to shock glass, the fusion crust is a brown, bubble-rich glass (Fig. 3d).

The mineral modes are comparable with the rough estimates given for SaU 005/008 (Zipfel, 2000; Table 1). The mineral modes, especially the high amount of olivine, are similar to Dar al Gani (DaG) 476/489/670/735 (Folco *et al.*, 2000; Mikouchi *et al.*, 2001; Zipfel *et al.*, 2000; Wadhwa *et al.*, 2001) with the exceptions that phosphates are very rare and no mesostasis containing Fe-rich olivine was found (Table 1). The high abundance of olivine and the slightly zoned mineralogy indicate affinities to lherzolitic shergottites (*e.g.*, Gleason *et al.*, 1997; Harvey *et al.*, 1993; Treiman, 1990). Without considering the shock melt, thin section SaU 094C contains >90 vol% mafic minerals (Table 1). SaU 094 thus takes an intermediate position between mafic and ultramafic shergottites, and according to its mineral mode and grain size has to be classified as melanocratic olivine microgabbro with transitions to olivine clinopyroxenite (Streckeisen, 1976). Grain size and texture are similar to terrestrial doleritic dikes/sills or microgabbroic intrusions.

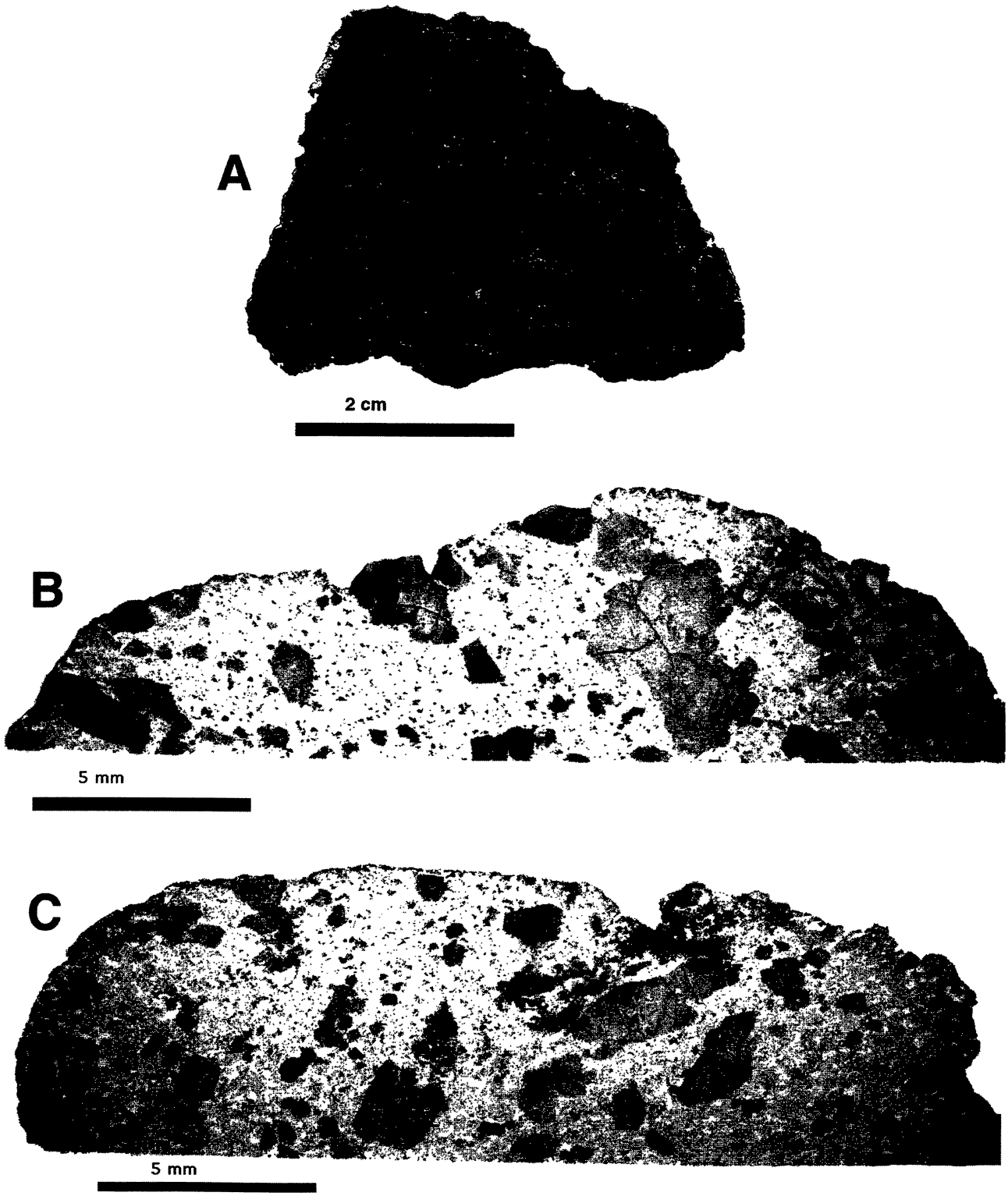

FIG. 1. (a) Slice of SaU 094. Dark patches are olivine crystals and local impact melt; the lighter areas consist of clinopyroxene and maskelynite. Images (b) and (c) are two thin sections cut perpendicular to the surface and used for point-counting and microprobe analyses. Larger crystals are olivine. Dark areas are finely-crystallized zones rimming green shock glass.

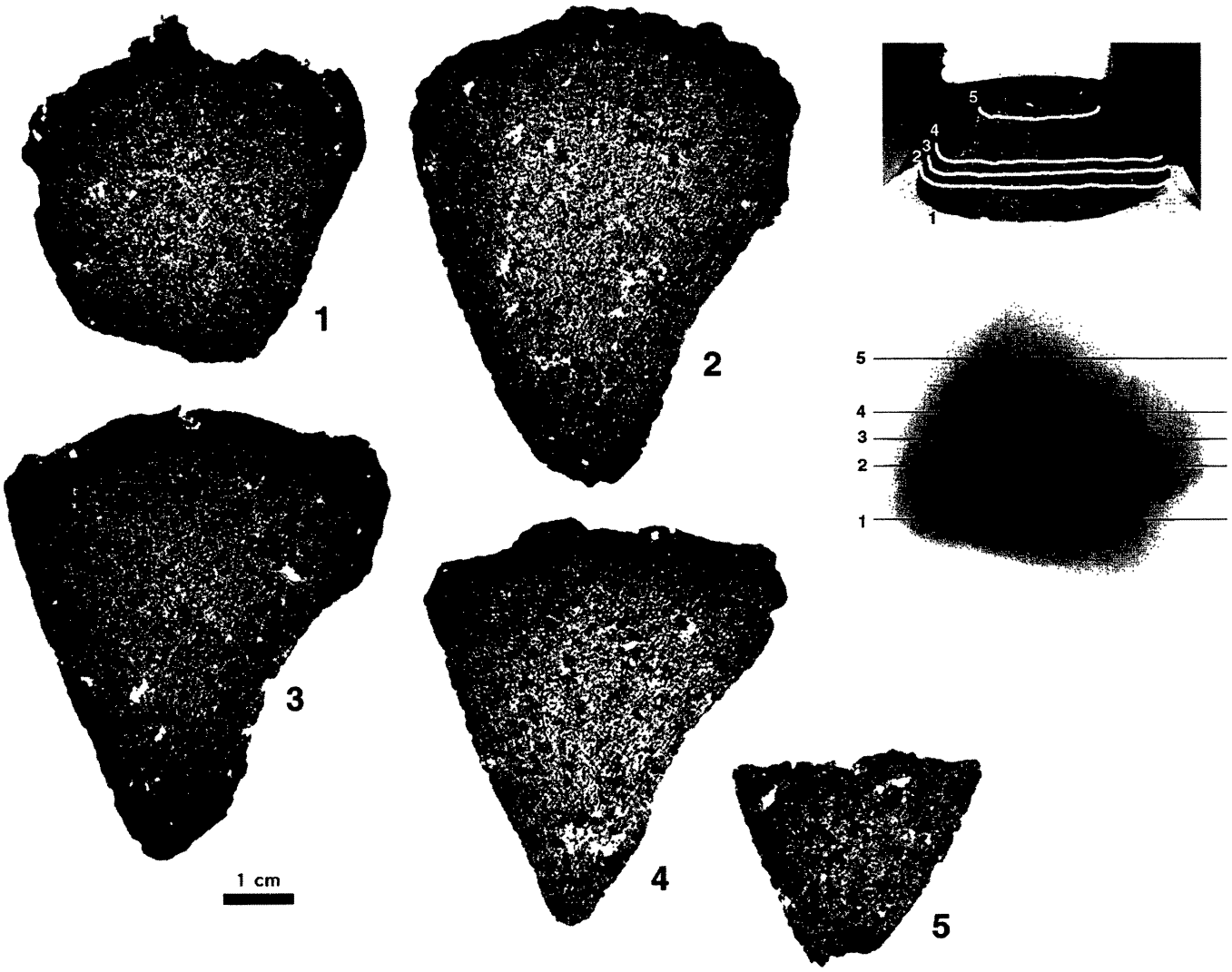

FIG. 2. X-ray tomograms of SaU 094 made at the Federal Institution for Material Research, Dübendorf, before cutting the rock. The top right image shows the stone in analysis position with the traces of the five parallel tomographs. The image below shows the same sections on a transmission x-ray image taken at a right angle relative to the tomographs. Numbers refer to the tomographic sections. Original pixel size of the x-ray images is 0.1 mm. Dark areas are olivines, gray areas correspond to the groundmass (including shock melts) and the white areas are vesicles in melt pockets.

FIG. 3. (*right*) Photomicrographs of SaU 094. (a) Microgabbroic texture consisting of millimeter-sized olivine crystals set in a groundmass of prismatic pigeonite and maskelynite. Transmitted light, section D, width of image 3.8 mm. (b) Olivine crystal containing abundant small melt inclusions (darker patches) characteristically surrounded by radial cracks. Section C, width of image 1.4 mm. (c) Pocket of green impact glass with orbicular and elongated vesicles and flow structures in unhomogenized melt. Along the pocket boundary the melt is crystallized into feathery crystals of both clinopyroxene and olivine. Crossed polarizers, section D, width of image 0.5 mm. (d) Thick rim of bubble-rich glassy fusion crust. Note the sharp boundary of the darker fusion crust (top) to the lighter impact glass that contains feather-like crystals. Section D, width of image 0.5 mm. (e) Zoned chromite grain with speckled Cr-rich core and ulvöspinel-enriched rim (see Fig. 6i). Dark area in center is a magmatic melt inclusion. Reflected light, oil immersion, section D, base of image 0.16 mm. (f) Pyrrhotite showing coarse granular pentlandite (lighter area) and small pentlandite exsolutions lamellae. Associated platy oxide grains on top are ilmenite, on the left chromite. Reflected light, oil immersion, section C, width of image 0.09 mm. (g) Bright orange secondary Mg-Fe-Si silicate (Alt) found in association with melted areas. Its mineralogic composition is unknown. Plain polarized light, section D, width of image 0.5 mm. (h) Scanning electron image of vesicle in impact melt glass containing gypsum crystals, probably derived from alteration of sulfide during martian or terrestrial alteration. Width of image 145 μm.

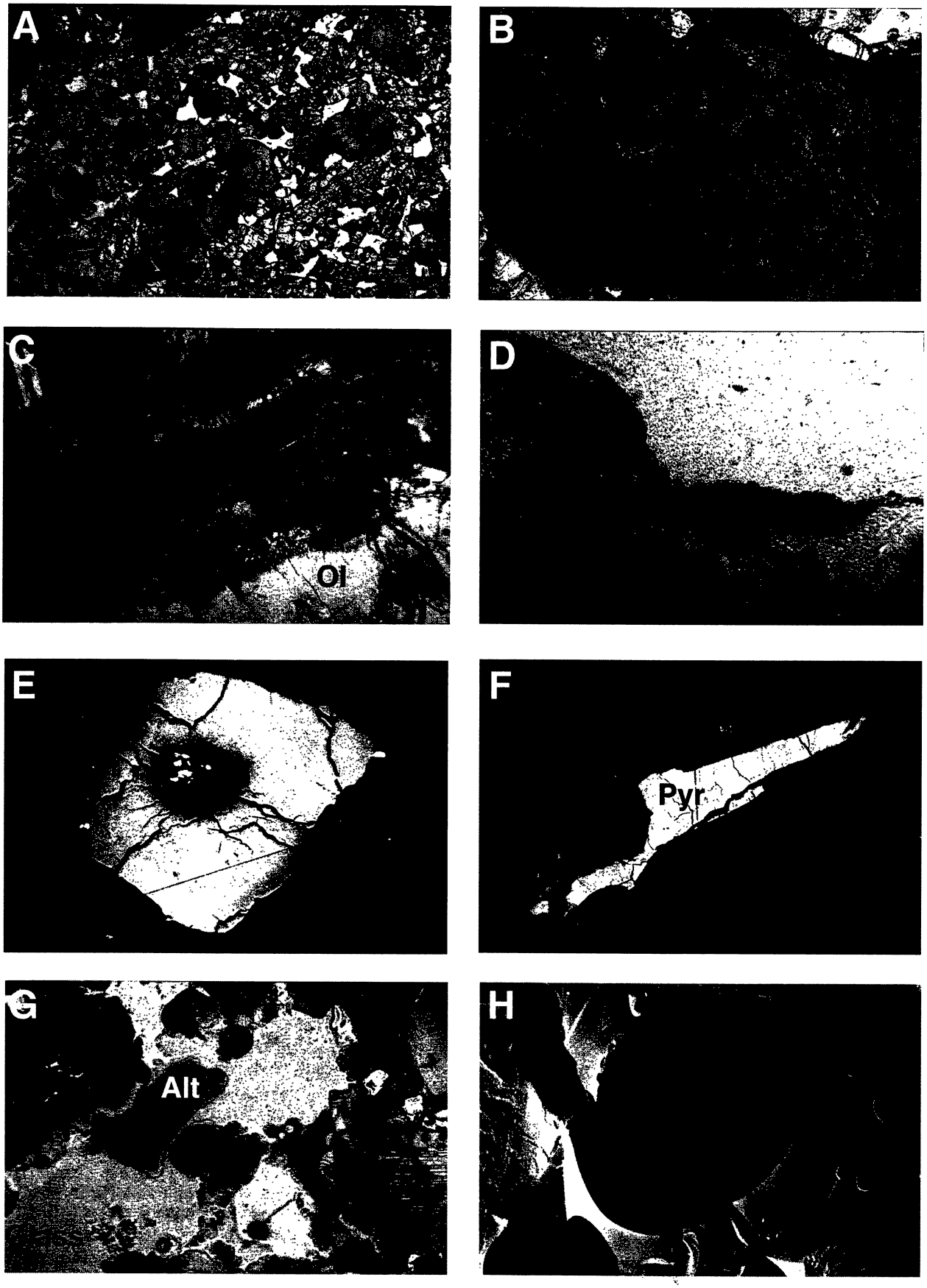

TABLE 1. Modal composition of SaU 094 compared with other martian meteorites.

Meteorite	SaU 094 (n = 1300) (section C)	SaU 094 (n = 1300) (section D)	SaU 005 and 008*	DaG 476 and 489†	EETA79001A‡	LEW 88516§
Lithology	Olivine clinopyroxenite#	Gabbro	Basalt@	Basalt@	Basalt@	Lherzolite@
Pyroxene (total)	**52.0**	**58.2**	**~48**	**55.3–64.6**	**69–73**	**>20–44.5**
Pigeonite				44.1–53-?	55–63	
Augite				2.9–12.7	3.2–8.5	
Orthopyroxene				1.5–4.0	3.4–7.2	
Olivine (total)	**31.0**	**22.1**	**~25**	**10.4–24**	**7–10**	**39.2–57**
dark	3.7	1.6				
light	27.3	20.5				
Maskelynite	**8.6**	**13.7**	**~15**	**12–17**	**16–18**	**<10–16**
Opaques	**1.1**	**1.1**		**0.9–3.9**	**2.2–4.0**	**<5**
Chromite	0.9	1.0		0–0.6		0.8–3
Ilmenite	tr	tr				
Pyrrhotite	0.2	0.1		0–0.6		<1
Merrillite	**tr**	**tr**		**tr–1.5**	**tr–0.4**	**0.9–1**
Mesostasis				–	**tr–0.3**	
Impact glass	**6.7**	**4.8**	**~9**	**4–7.2**	–	–
Unaltered glass	2.7	0.7				
Recryst glass	4.0	4.1				
Primary inclusions	**0.6**	**0.1**				
Alteration minerals	**tr**	**tr**	–	**1–3.1**	–	–
"Shock cavities"	**(0.4$)**	**(0.4$)**				

*Zipfel (2000).
†Zipfel *et al.* (2000); Folco *et al.* (2000); Wadhwa *et al.* (2001); Mikouchi *et al.* (2001).
‡McSween and Jarosewich (1983).
§Gleason *et al.* (1997); Treiman *et al.* (1994); Lodders (1998).
#Two out of 1300 points are red alterations in glass; if impact melt is not included and opaques substracted the rock contains 8.9 vol% maskelynite.
$Shock cavities point-counted on x-ray tomography images (Fig. 2); not present in the two point-counted thin sections.
@As described by authors.
Abbreviations: tr = trace.

Chromite grains are isometric, opaque to brownish translucent and show an average maximum diameter of 0.10 mm. In reflected light (oil immersion) they commonly show a slightly browner Ti-rich rim (Fig. 3e). Intergrowths with ilmenite are common. 5–10 μm sized, isometric chromite inclusions are characteristic in the cores of some olivines. Chromite grains rarely show inclusions of sulfides. Ilmenite typically occurs as laths showing lamellar twinning (Fig. 3f) and is often associated with chromite and sulfides.

Merrillite occurs in trace amounts and was only found using the cathode luminescence technique, where it shows a yellow color. The grains are isolated and occur associated with maskelynite and along olivine rims.

Sulfide grains (average maximum dimension 0.07 mm) are commonly elongated and consist of polycrystalline pyrrhotite carrying two types of pentlandite inclusions: type 1 are hypidiomorphic crystals up to 10 μm in size (Fig. 3f); type 2 are tiny (>1 to 2 μm) oriented exsolutions (Fig. 3f; see also Fig. 9). Image analysis of nine high-magnification photomicrographs indicates the presence of 8.5 ± 2.5 vol% pentlandite in the sulfides. In areas where the rock was shock-melted, pyrrhotite forms granular globules (8.4% of sulfide grains) also containing pyrrhotite (incomplete shock-melt?). Pyrrhotite may fill small cracks (3.2% of sulfide grains) in the silicates, and also occurs in melt inclusions in olivine (1.2% of sulfide grains). Investigation of pyrrhotite using a magnetic colloid (Bitter method; Soffel, 1991) showed that pyrrhotite is dominantly non-magnetic. Magnetic areas of very small size were only observed in close association with nearby weathering products, indicating a possible oxidation-related origin of the small amounts of magnetic pyrrhotite present.

Oval-shaped multiphase melt inclusion are common in olivine characteristically surrounded by radial cracks in the host mineral (Fig. 3b). The size of the inclusions is below 0.1 mm. Qualitative data show that the melt inclusions contain Ca-rich clinopyroxene, spinel, pyrrhotite, and a glassy silicate matrix.

Although the inclusions appear similar to those described by Goodrich and Zipfel (2001) from SaU 005, the microprobe beam could not be sufficiently focused to obtain proper single phase analyses.

In thin section, millimeter to centimeter-sized pockets of a green shock glass are observed. The green glass characteristically contains gas bubbles or vesicles that may reach several millimeters (Figs. 2 and 3c). At the contact to the surrounding silicates a dark brown to black zone occurs characterized by crystallization of acicular and commonly skeletal olivine or clinopyroxene crystals (Fig. 3c,d). Sulfide droplets and rounded (partially melted) chromite grains are common. Around melt pockets olivine and pyroxene show textures suggesting that parts of the grains were melted and subsequently recrystallized into a fine-grained zone largely with conservation of the original grain shape. The refractive index of four green glass fragments is 1.634–1.638, with some variation within one grain. Considering that some melt pockets in olivine- or pigeonite-dominated areas have a very different composition (Table 2), the obtained values probably do not represent the full range of shock glass refractive indices. In the section investigated the shock glass shows no luminescence but in the recrystallized fine-grained parts a weak orange to reddish luminescence of unknown origin is locally observed.

The rock contains ~0.4% of millimeter-sized vesicles forming the central part of millimeter to centimeter-sized shock melt pockets. The five x-ray tomographs taken parallel to each other (Fig. 2) revealed that these vesicles, and conceivably also the melt pockets, have an elongated shape and show a preferred orientation (Fig. 4). The smallest vesicles (<<1 mm) are spherical in shape (Fig. 3c).

The calculated density is 3.309 g cm^{-3} with vesicles excluded and 3.296 g cm^{-3} with 0.4 vol% vesicles included. The measured density of a 16 g piece is 3.226 g cm^{-3}. The measured value is probably slightly lower due to microporosity.

Products of terrestrial weathering are present throughout the meteorite in minor amounts. Calcite veinlets are especially common in a 3–10 mm thick zone at the surface of the meteorite (see vein crossing the vesicle in Fig. 3c). Some calcite veins clearly crosscut the locally preserved fusion crust. Patches of Fe hydroxide, most likely of terrestrial weathering origin, occur throughout the meteorite as fillings of tiny cracks and as small pockets of finely layered oxidation products of an unidentified phase or mix phases (Fig. 3g). Pyrrhotite usually shows no sign of oxidation; however, rare grains even in the meteorite's interior are strongly oxidized with partial alteration to marcasite and Fe-hydroxides. In vesicles Fe-hydroxides, fine-grained (<1 μm) calcite and fine-grained to coarse idiomorphic gypsum (Fig. 3f) were identified as common alteration products.

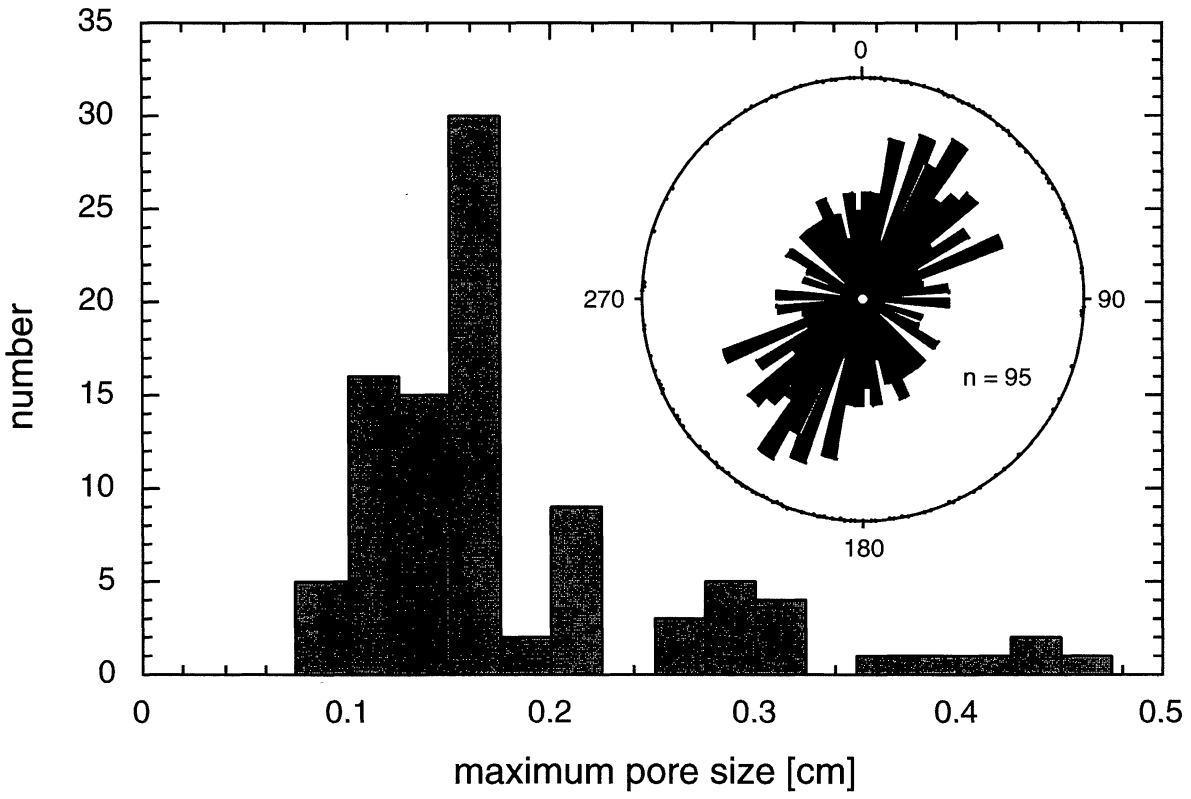

FIG. 4. Histogram of vesicle size (maximum length) and vesicle orientation obtained from the five parallel x-ray tomographs (Fig. 2). Note the clear preferred orientation of the vesicles in SaU 094 shown in the rose diagram.

TABLE 2. Shock melt and fusion crust glasses in SaU 094.

Sample	Shock glass					Fusion crust		Mafic shergottites		Ultramafic shergottites			
	SaU 094D Pocket 1	SaU 094D Pocket 2	SaU 094D Pocket 3	Range	Range (except pocket D3)	SaU 094C #4*	Range	SaU 094_{calc}†	SaU 005‡	DaG 476§	ALH 77005#	LEW 88516#	Y-793605#
SiO_2	47.72	54.00	38.05	38.05–54.00	47.72–54.00	48.49	48.04–49.07	48.66	47.20	48.91	42.36	46.00	45.35
TiO_2	0.34	0.14	0.02	0.03–0.45	0.14–0.45	0.41	0.36–0.44	0.26	0.42	0.42	0.39	0.39	0.35
Cr_2O_3	1.01	0.56	0.04	0.04–1.65	0.56–1.65	1.03	0.73–1.03	0.99	0.78	0.83	0.97	0.86	1.01
Al_2O_3	2.60	1.001	0.04	0.02–3.68	1.00–3.68	4.97	4.22–5.25	4.12	4.53	4.67	2.87	3.31	2.32
FeO_{tot}	19.48	15.88	30.06	15.19–30.48	15.19–19.50	16.34	16.34–18.11	17.96	18.07	17.17	20.07	19.04	19.68
MnO	0.42	0.493	0.54	0.41–0.64	0.41–0.64	0.43	0.40–0.54	0.50	0.46	0.48	0.45	0.49	0.48
MgO	23.40	23.28	31.49	21.81–31.63	21.81–23.60	20.54	20.31–22.01	22.73	20.49	20.75	28.19	24.95	26.20
NiO	b.d.	b.d.	b.d.	b.d.–0.13	b.d.–0.13	b.d.	b.d.–0.15	–	–	–	–	–	–
CoO	–	b.d.	0.05	b.d.–0.08	b.d.–0.08	b.d.	b.d.–0.12	–	–	–	–	–	–
CaO	4.44	4.53	0.32	0.31–5.50	4.21–5.50	5.62	5.22–5.73	4.52	5.46	5.84	3.16	4.20	4.06
Na_2O	–	0.11	b.d.	b.d.–0.45	0.14–0.45	0.64	0.12–0.74	0.55	0.60	0.55	0.47	0.57	0.35
K_2O	–	–	–	–	–	–	–	b.d.	b.d.	0.04	0.03	0.03	0.02
SO_2	0.09	b.d.	b.d.	b.d.–0.25	b.d.–0.25	0.02	b.d.–0.03	–	–	–	–	–	–
Total	99.50	99.99	100.61	99.13–101.45	99.13–100.81	98.49	98.76–100.18	100.29	98.01	99.66	98.96	99.84	99.82

*Analysis number.
†Calculated using mineral modes (Table 1) and average microprobe analyses.
‡Dreibus *et al.* (2000).
§Zipfel *et al.* (2000).
#Lodders (1998); recalculated as oxides.
Abbreviations: b.d. = below detection limit, – = not analyzed.

MINERAL, SHOCK AND FUSION GLASS CHEMISTRY

Olivine has a restricted compositional range of Fo_{65-69} (Table 3; Fig. 5a). The olivines average 0.56 wt% MnO, are relatively high in CaO (0.37 wt%) and contain little NiO (0.03 wt%) and Cr_2O_3 (0.06 wt%). The average FeO/MnO is 51.9 ± 3.4. Increasing shock oxidation is correlated with an increased ferrifayalite (laihunite component) of the olivine (Fleischer *et al.*, 1978; Ostertag *et al.*, 1984), manifested in reduced microprobe totals (Table 3) and darker brown color. The amount of ferric iron (laihunite component; $Fe^{3+}{}_2\square_1Fe^{2+}{}_{-3}$-exchange) in the olivines was estimated by normalizing to 1 Si (pfu). Microprobe traverses (Fig. 6a,b) revealed zoning similar to the zoning described by Mikouchi *et al.* (2001) for DaG 476, but less pronounced.

Pigeonite ($En_{60-68}Fs_{20-27}Wo_{7-9}$) shows relatively restricted compositional variation (Table 3; Fig. 5b). No enstatite was detected. Augite ($En_{46-49}Fs_{15-16}Wo_{28-31}$) occurs rarely associated with the pigeonite and is listed in Table 3. In backscattered electron images weak pyroxene zoning is visible, and no exsolution of pigeonite into enstatite and augite was observed. Qualitative analyses show that pyroxene in melt inclusions has distinct higher Al values (4–5 wt% Al_2O_3) than the matrix pyroxene (average 1.21 ± 0.43). Pigeonite microprobe traverses (Fig. 6c,d) are characteristically flat and irregular due to shock deformation and possible exsolution.

The clear maskelynite glass filling the interstitial areas between olivine and pyroxene grains seems stoichiometric and has a labradoritic composition ($An_{50-64}Or_{0.3-0.9}$; Fig. 5c) with relatively high potassium contents (Table 3). In one case (Fig. 6f) anorthite content dropped to 50%. The maskelynite also contains measurable amounts of Fe, Mn and Mg (Table 3). Maskelynite microprobe traverses are generally flat (Fig. 6e) but in one case a continuous change towards one rim was detected (Fig. 6f).

Chromites to titanian magnesian chromites contain 0.1–0.3 wt% ZnO, 1.0–15.2 wt% TiO_2, 3.9–5.1 wt% MgO and 7.9–11.9 wt% Al_2O_3 (Table 4). They form subhedral grains and clusters occurring in association with all other minerals (*e.g.*, Fig. 3e). Chromites show considerable variation in Ti content. If the ulvöspinel vector, $M^{2+}Ti^{4+}\ M^{3+}{}_{-2}$, is plotted (Fig. 7a), a perfect relationship is obtained with Mg (magnesioulvöspinel) the most important divalent, and Cr the main trivalent cation ($Mg^{2+}Ti^{4+}\ Cr^{3+}{}_{-2}$). Two microprobe traverses (Fig. 6i,k) show ulvöspinel-enriched rims and asymmetric zoning.

Ilmenite (Ilm_{80-86}; 6% of dark opaques) contains up to 0.7 wt% MnO (pyrophanite component), up to 4.7 wt% MgO (geikielite) and up to 0.48 wt% Cr_2O_3 (eskolaite). Ilmenites are plotted together with the chromites in Fig. 7b, and an analysis listed in Table 4.

All phosphate grains found are merrillite $Ca_9Na(Mg,Fe)(PO_4)_7$ (Dowty, 1977). Similar to other martian meteorites (*e.g.*, Mikouchi *et al.*, 2001) merrillite contains considerable amounts of F (average 1.1 wt%), and traces of Cl

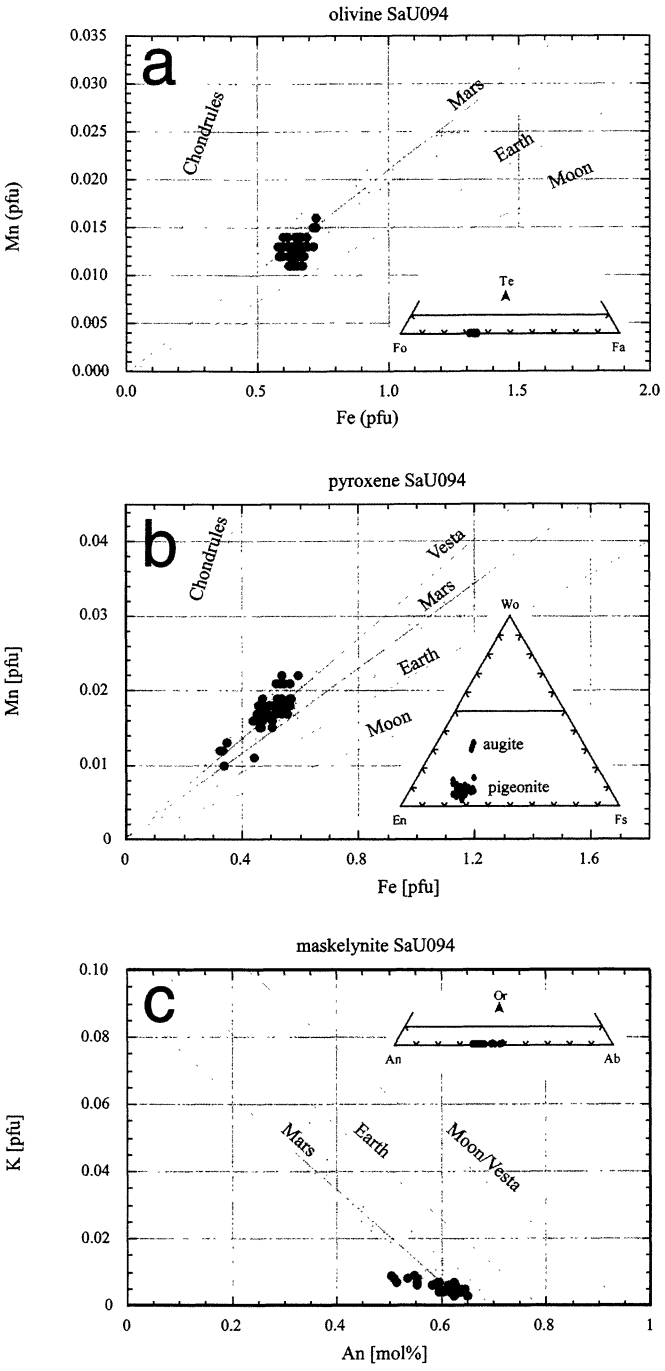

FIG. 5. Fe-Mn compositions of olivine and clinopyroxene and anorthite-K compositions of maskelynite in SaU 094 compared to compositional trends (lines and shaded areas) given by Papike (1998). Insets show compositions in the corresponding ternary diagrams. Te = tephroite.

(Table 5) which point to either solid-solution with a structurally similar "fluor whitlockite" or, as replacement of PO_4 by SiO_4 suggests, a solid-solution series with structurally similar silicate members (*e.g.*, Moore, 1983). Rare earth elements are only present in trace amount and at the limit of detection by

TABLE 3. Silicates in SaU 094B.

	Olivine					Augite	Pigeonite				Maskelynite			
Analysis	#1	#6	#13	#18	Range	#15	#5	#10	#26	Range	#1	#2	#4	Range
SiO_2	37.77	37.41	37.06	37.47	36.68–37.97	53.22	54.18	54.19	52.56	52.06–54.39	54.99	53.00	52.73	52.35–54.99
TiO_2	b.d.	b.d.	b.d.	b.d.	b.d.	0.32	0.12	0.06	0.23	0.06–0.91	b.d.	b.d.	b.d.	b.d.
Cr_2O_3	0.04	0.08	0.07	0.03	0.02–0.60	0.83	0.51	0.47	0.55	0.25–1.29	0.03	0.03	0.03	0.03
Al_2O_3	0.04	0.04	0.11	0.08	0.01–0.21	2.10	1.00	1.14	1.75	0.67–1.98	28.24	29.51	29.97	28.16–29.97
Fe_2O_3	–	–	–	–	–	0.45	1.13	0.49	1.18	0.16–3.83	0.00	0.00	0.00	0.00–0.66
FeO	26.63	28.43	27.23	27.37	25.83–31.98	10.52	13.98	14.56	14.59	10.79–18.13	0.37	0.43	0.39	0.00–0.52
Mn0	0.53	0.54	0.53	0.77	0.46–0.71	0.38	0.56	0.57	0.56	0.50–0.69	0.02	0.04	0.00	0.00–0.04
MgO	34.75	32.90	30.94	30.80	30.14–34.75	17.90	24.78	25.30	21.99	21.75–25.30	0.12	0.15	0.16	0.12–0.61
NiO	b.d.	b.d.	b.d.	b.d.	b.d.–b.d.	0.05	b.d.	b.d.	b.d.	b.d.–0.04	b.d.	b.d.	b.d.	b.d.
CaO	0.42	0.34	0.57	0.79	0.29–0.88	15.72	4.49	3.48	6.46	3.48–6.89	11.32	12.85	13.14	11.32–13.14
Na_2O	b.d.	b.d.	b.d.	b.d.	b.d.–b.d.	0.19	0.08	0.03	0.09	b.d.–0.11	5.07	4.16	3.96	3.96–5.07
K_2O	b.d.	b.d.	b.d.	b.d.	b.d.–b.d.	b.d.	0.02	b.d.	b.d.	b.d.–0.04	0.15	0.09	0.09	0.06–0.15
Total	100.18	99.74	96.51	97.31	96.11–100.95	101.68	100.85	100.29	99.96	99.20–100.89	100.31	100.26	100.47	99.74–100.69
Si	1.000*	1.000*	1.000*	1.000*	1.000*	1.935	1.956	1.962	1.935	1.900–1.970	2.478	2.401	2.386	2.384–2.550
Ti	b.d.	b.d.	b.d.	b.d.	b.d.	0.009	0.003	0.002	0.007	0.002–0.025	b.d.	b.d.	b.d.	b.d.–0.004
Cr	0.001	0.002	0.001	0.001	b.d.–0.013	0.024	0.015	0.014	0.016	0.007–0.037	0.001	0.001	0.001	b.d.–0.002
Al	0.001	0.001	0.003	0.003	b.d.–0.007	0.090	0.043	0.049	0.076	0.029–0.086	1.500	1.575	1.598	1.430–1.598
Fe^{III}	0.026	0.058	0.213	0.239	b.d.–0.243	0.012	0.031	0.013	0.033	0.005–0.105	–	–	–	–
Fe^{II}	0.564	0.577	0.413	0.368	0.367–0.756	0.320	0.422	0.441	0.449	0.329–0.559	0.014	0.016	0.015	b.d.–0.044
Mn	0.012	0.012	0.011	0.010	0.010–0.016	0.012	0.017	0.018	0.017	0.016–0.022	0.001	0.002	b.d.	b.d.–0.002
Mg	1.371	1.311	1.245	1.227	1.214–1.371	0.970	1.333	1.365	1.207	1.190–1.367	0.008	0.010	0.011	0.007–0.096
Ni	b.d.	b.d.	b.d.	b.d.	b.d.	0.002	b.d.	b.d.	b.d.	b.d.–0.001	b.d.	b.d.	b.d.	b.d.
Ca	0.012	0.010	0.016	0.025	0.008–0.025	0.612	0.174	0.135	0.255	0.135–0.269	0.547	0.624	0.637	0.500–0.637
Na	b.d.	b.d.	b.d.	b.d.	b.d.	0.014	0.006	0.002	0.007	b.d.–0.008	0.443	0.365	0.347	0.347–0.485
K	b.d.	b.d.	b.d.	b.d.	b.d.	0.001	0.001	b.d.	b.d.	b.d.–0.002	0.009	0.005	0.005	0.003–0.009
Fo†	0.695	0.670	0.662	0.666	En	0.507	0.680	0.699	0.621	An	0.548	0.628	0.644	
Fa	0.299	0.324	0.333	0.329	Fs	0.173	0.231	0.232	0.248	Ab	0.443	0.367	0.351	
Te‡	0.006	0.006	0.006	0.005	Wo	0.320	0.089	0.069	0.131	Or	0.009	0.005	0.005	

Abbreviations: b.d. = below detection limit; – = not analyzed.
*Normalized to 1 Si per formula unit; Fe^{3+} is calculated according to discussion in text.
†Fo = Mg/Mg + Fe_{tot} + Mn.
‡Te = tephroite.

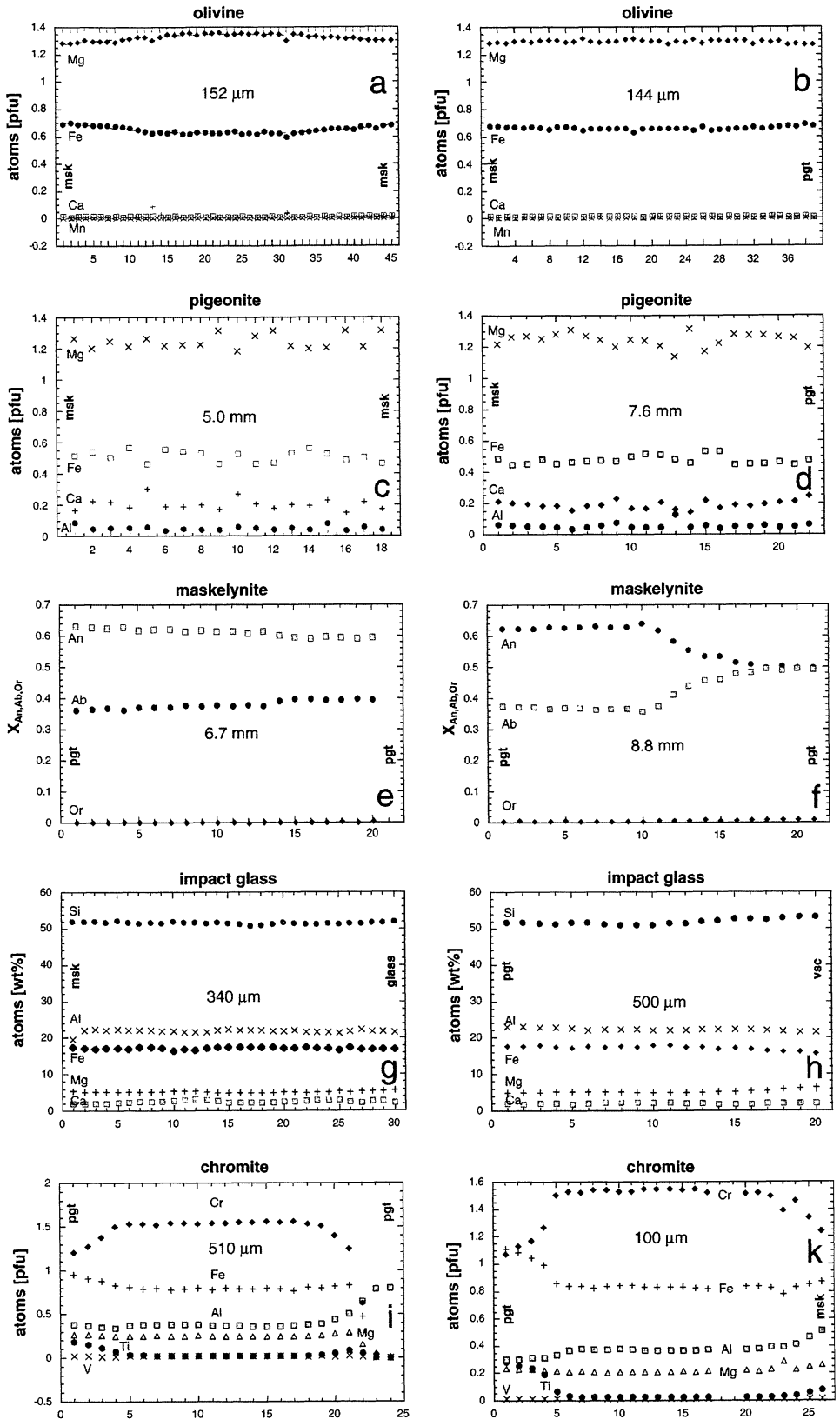

FIG. 6. Mineral transects displaying weak to absent chemical zoning; numbers indicate analysis spots. Abbreviation are phases in contact with the analyzed grain: msk = maskelynite; pgt = pigeonite; glass = recrystallized glass; vsc = vesicle.

TABLE 4. Oxides in SaU 094.

	Chromite				Ilmenite
Sample	SaU 094C	SaU 094C	SaU 094B		SaU 094B
Analysis	#17	#59	#21	Range	#43
SiO_2	0.09	0.17	0.03	0.02–0.79	0.04
TiO_2	0.70	1.03	15.22	0.46–15.22	53.31
Cr_2O_3	60.58	56.58	31.03	31.03–61.05	0.48
V_2O_3	0.52	0.73	–	0.29–0.82	–
Al_2O_3	6.95	9.27	5.99	5.99–17.68	b.d.
Fe_2O_3	–	–	2.17	(b.d.–3.20)	0.40
FeO_{tot}	26.23	27.58	40.41	26.72–40.41	41.50
MnO	b.d.	b.d.	b.d.	b.d.	0.74
MgO	4.60	4.83	4.14	3.63–5.40	3.11
ZnO	0.27	0.11	0.14	b.d.–0.33	–
NiO	0.08	0.13	0.12	b.d.–0.19	b.d.
CoO	b.d.	b.d.	b.d.	b.d.–0.11	–
CaO	b.d.	b.d.	0.09	0.01–0.32	0.15
Total	100.02	100.43	99.34	99.32–100.92	99.73
Si	0.003	0.006	0.001	0.001–0.021	0.001
Ti	0.018	0.027	0.408	0.021–0.408	0.991
Cr	1.665	1.533	0.874	0.874–1.604	0.009
Al	0.285	0.374	0.251	0.251–0.688	b.d.
Fe^{3+}	b.d.	0.007	0.058	0.022–0.084	0.008
Fe^{2+}	0.762	0.781	1.263	0.810–1.263	0.858
Mn	b.d.	b.d.	b.d.	b.d.	0.015
Mg	0.239	0.247	0.220	0.189–0.273	0.115
Zn	0.007	0.003	0.004	b.d.–0.008	–
Ni	0.002	0.004	0.003	b.d.–0.005	b.d.
Co	b.d.	b.d.	b.d.	b.d.	–
Ca	0.001	0.001	0.003	b.d.–0.012	0.004

Abbreviations: – = not analyzed, b.d. = below detection limit.

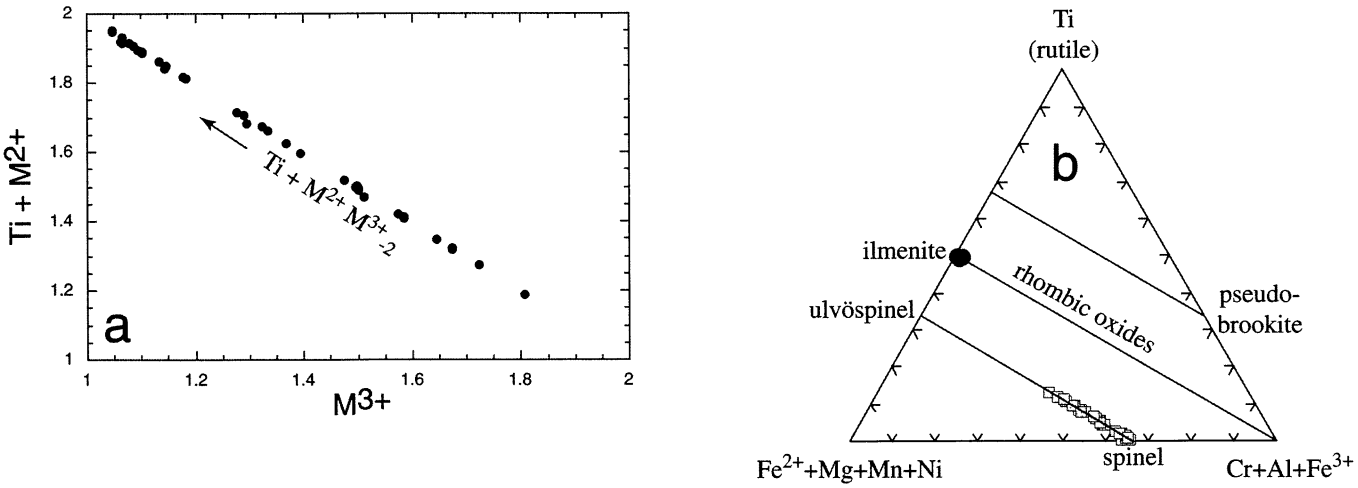

FIG. 7. Chromite (a, b) and ilmenite (b) compositions in SaU 094.

TABLE 5. Phosphates and sulfides in SaU 094.

	Merrillite				Pyrrhotite			Sulfide melt	Pentlandite
Sample	SaU 094B	SaU 094B	Range		SaU 094C	SaU 094C	Range	SaU 094C	SaU 094C
Analysis	#9	#20			#2	#28		#17	#3
P_2O_5	44.77	45.64	42.75–45.64	Cr	b.d.	b.d.	b.d.0–0.54	0.07	b.d.
SiO_2	1.38	0.36	0.36–1.64	Fe	60.47	55.85	55.37–63.04	63.04	37.21
Al_2O_3	0.23	0.10	0.09–0.47	Mn	0.06	b.d.	b.d.–0.07	0.10	0.03
FeO	1.17	1.10	0.85–1.28	Zn	b.d.	0.19	b.d.–0.21	b.d.	b.d.
MgO	4.04	3.56	3.50–4.61	Ni	2.19	4.13	0.73–7.20†	0.45	29.17
CaO	46.15	47.22	46.03–47.60	Co	0.03	0.10	b.d.–0.10	0.14	0.66
Na_2O	1.75	1.71	1.48–1.86	Cu	b.d.	b.d.	b.d.–1.11	b.d.	b.d.
Ce_2O_3	b.d.	b.d.	b.d.–0.06	Se	0.05	0.03	b.d.–0.08	b.d.	0.06
La_2O_3	b.d.	0.04	b.d.–0.07	As	0.04	0.04	b.d.–0.09	b.d.	0.05
Nd_2O_3	0.08	b.d.	b.d.–0.08	S	37.01	37.22	36.44–38.09	36.08	33.42
Y_2O_3	0.09	0.04	0.03–0.09						
F	1.16	1.05	0.50–1.28						
Cl	0.09	b.d.	0.02–0.10						
Total	100.31*	100.32*	99.18–100.44*	Total	99.85	99.56	99.03–100.92	99.88	100.60
P	6.795	6.933	6.575–6.933	Cr	b.d.	b.d.	b.d.–0.009	0.001	0.004
Si	0.248	0.065	0.065–0.297	Fe	0.938	0.893	0.843–0.965	1.003	5.110
Al	0.048	0.021	0.020–0.100	Mn	0.001	b.d.	b.d.–0.002	0.002	0.003
Fe	0.175	0.165	0.128–0.191	Zn	b.d.	0.003	b.d.–0.003	b.d.	b.d.
Mg	1.080	0.953	0.949–1.243	Ni	0.032	0.061	0.011–0.108	0.007	3.812
Ca	8.865	9.077	8.826–9.317	Co	b.d.	0.001	b.d.–0.001	0.002	0.086
Na	0.607	0.596	0.523–0.645	Cu	b.d.	0.008	b.d.–0.008	b.d.	b.d.
Ce	b.d.	0.001	b.d.–0.013	Se	0.001	b.d.	b.d.–0.001	b.d.	0.006
La	b.d.	0.003	b.d.–0.005	As	b.d.‡	0.001‡	b.d.–0.001‡	b.d.‡	0.005‡
Nd	0.005	b.d.	b.d.–0.014	S	1.000‡	0.999‡	0.999–1.000‡	1.000‡	7.995‡
Y	0.008	0.004	0.004–0.008						
F	0.656	0.598	0.289–0.739						
Cl	0.028	0.005	0.005–0.030						

Abbreviations: b.d. = below detection limit. Detection limits at the 2σ level were derived in the following way: (2σ) in ppm = $10^4 \times 2.241/(t_{tot} \times I_{pk} \times I_{pk}/I_{bdg})^{1/2}$ where t_{tot} = total integration time in seconds, I_{pk} = intensity on pure peak in counts per second, and I_{bgd} = intensity on background in counts per second. Detection limits in ppm are: Ce, 200; La, 200; Nd, 450; Y, 250. Detection limits for Se and As in the sulfides are 250 ppm. Relative 1σ analytical uncertainties for these elements are 50–250%.

*Corrected for F, Cl = O.

†Maximum value where only small exsolutions occur.

‡Normalized to the elements marked.

microprobe. Yttrium is dominating, pointing to a heavy REE enrichment.

The iron sulfide chemistry varies between FeS (troilite) and $Fe_{10}S_{11}$ (hexagonal non-magnetic pyrrhotite; Craig and Scott, 1974) with Fe/S ratios between 0.92 to 1.00 (Table 5). Pyrrhotite also contains small amounts of Cr and Co (Table 5). Due to the presence of irregularly distributed pentlandite inclusions (Fig. 3; see also Fig. 9), pyrrhotite analyses show a wide range of NiS contents of 0.9–7.2 wt% (Table 5). Areas free of pentlandite exsolution typically contain 2.7–3 wt% Ni. Arsenic and selenium are found to be at the detection limit, but pentlandite (Table 5) seems to concentrate selenium.

The green shock glass pockets interpreted as shock-induced melts have, according to the total alkalies *vs.* silica classification (Le Maitre *et al.*, 1989), mainly a basaltic to basaltic andesite composition (Fig. 8). Compared with a bulk analysis of SaU 005 (Dreibus *et al.*, 2000; Table 2), the shock glass is commonly enriched in SiO_2, possibly due to partial recrystallization to relatively Si-poor phases (*e.g.*, olivine). The glass composition of the largest pocket analyzed plots close to the SaU 005 bulk composition (Fig. 8). However, the compositions of a few small melt pockets strongly deviate from the bulk composition, reflecting local melting of minerals (Table 2). Microprobe profiles across two larger melt pockets (Fig. 6g,h) revealed no

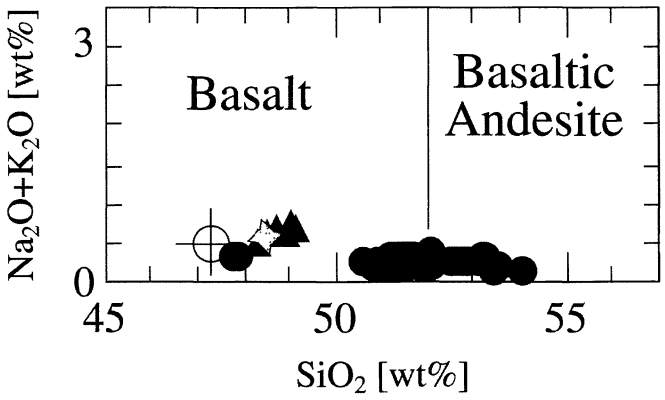

FIG. 8. Chemical compositions of impact glass (circles), fusion crust (triangles), bulk composition calculated from microprobe mineral averages and mode (star), and SaU 005 bulk composition (circle with cross; Dreibus *et al.*, 2000) plotted in the TAS classification diagram for volcanic rocks (Le Maitre *et al.*, 1989). Note the similarity of fusion glass, larger melt pockets and calculated bulk composition with SaU 005. Some analyzed melt pocket glasses plot outside the diagram boundaries near 38 wt% SiO_2 (see Table 4).

zoning in the optically homogeneous green glass. The sulfur content is measurable but variable (Table 2).

Analyses of fusion crust glass are listed in Table 2 and shown in Fig. 8. Its composition is very similar to the bulk-rock chemistry of Dreibus *et al.* (2000). The brown color of the glass suggest the presence of ferric iron.

SHOCK FEATURES AND METAMORPHISM

SaU 094 is an unbrecciated, shocked gabbroic rock displaying solid-state deformation features as well as finely grained recrystallized areas along grain boundaries, and pockets of shock-melted rock (Fig. 3c).

In pyroxene mechanical shock deformation produced deformation bands, polysynthetic twin lamellae and fracturing. Polysynthetic mechanical twinning subparallel to (001) with twin spacing of 2–40 μm dominates in such a way that pigeonite appears like twinned magmatic plagioclase (Fig. 9a). The twin boundaries are generally straight, sometimes slightly curved. All pyroxene grains are irregularly fractured but one set of fractures perpendicular to the prism is common. Sets of planar fractures are restricted to areas around melt pockets. Along pyroxene grain contacts and within the crystals fine-grained granular corridors produced by frictional melting and recrystallization are very common (Fig. 9b).

Based on experimental calibrations that relate refractive index to shock pressure (*e.g.*, Stöffler, 1984) the optically isotropic, labradoritic maskelynite can be used for estimating minimum shock pressure in SaU 094. Refractive indices obtained for three maskelynite grains are 1.540 and twice 1.542, indicating shock pressures in excess of 45 GPa (Fig. 10).

Olivine is characteristically yellow to dark brown (Fig. 9c) and patchy and shows several sets of planar fractures and strong mosaicism (Fig. 9d). Locally, the grains were melted, the melt now visible as small crystalline grains and a bleached zone (deformation-free, recrystallized olivine) separating the oxidized olivine from the melt pocket (Figs. 3c and 10c). Areas and veins of fine-grained recrystallized olivine are common and quenched glassy olivine is locally preserved along melt pockets where olivine crystals turn clear (recrystallization to Fe^{2+}-olivine). At the contact to melt pockets olivine shows characteristically rounded (resorbed) edges.

Chromites behave brittly during shock metamorphism and show several sets of parallel fractures. The same is observed in the few phosphate grains. Compared with spinels, ilmenite shows more intense shock fracturing and characteristic mechanical twinning (Fig. 3e). Chromite and ulvöspinel are ideomorphic as inclusions in olivine and pyroxene, but rounded (resorbed) in contact with shock melt.

The most obvious shock feature in sulfide grains adjacent to silicate shock melts is complete or partial melting (Fig. 9e), resulting in the formation of globular sulfide droplets enclosing silicate droplets (Fig. 9f). One large pyrrhotite grain (Fig. 9f) shows partial melting and a recrystallized (grain size 5–10 μm), polygonal, pentlandite-free transition zone (50 μm wide) towards unaffected, pentlandite-rich, coarse polygonal pyrrhotite (grain size 20–50 μm). Pyrrhotite in the compositional range observed is hexagonal

FIG. 9. (*right*) Shock features in SaU 094. (a) Shock-induced mechanical twinning in pigeonite leading to a plagioclase-like appearance. Crossed polarizers, section D, width of image 1 mm. (b) Shock-produced fine-grained polygonal granular bands of recrystallized pigeonite in pigeonite. These bands characteristically occur at grain boundaries and commonly as parallel (crystallographically oriented?) swarms within pigeonite grains. Crossed polarizers, section D, width of image 1 mm. (c) Shock-oxidized olivine. At its left end, in the extension of the melt pocket, the olivine turns dark brown (higher defect density) and at the direct contact to the melt pocket the olivine is reduced due to *in situ* recrystalliation of the vitrified olivine. Plain light, section D, width of image 2 mm. (d) Olivine grain showing strong mosaicism. Crossed polarizers, section D, width of image 1 mm. (e) Maskelynite quenched in a state of being injected by brownish melt from left to right. Note the flow structures suggesting fluidization of maskelynite. Plane polarized light, section D, width of image 0.11 mm. (f) Pyrrhotite showing transition from coarse polygonal crystals (with pentlandite exsolution lamellae; right) to finer polygonal crystals with small silicate inclusions (center, dark speckles) to globular sulfide melt droplets set in silicate shock melt (left). Reflected light, oil immersion, section D, width of image 0.11 mm. (g) Globular sulfide melt droplets in silicate melt. Note that the sulfide melt droplets show exsolutions of silicate melt, and the silicate melt tiny exsolutions of sulfides. This suggests that maximum mutual solubility was reached. Reflected light, oil immersion, section D, width of image 0.09 mm. (h) Grano-globular partly-melted sulfide inclusion in melt pocket. Note the grain boundary areas full of silicate melt inclusions, whereas pentlandite exsolutions remain unaffected by melting in the central part of the grains. The sulfide aggregate was subsequently crossed by a carbonate vein. Reflected light, oil immersion, section D, width of image 50 μm. Msk = maskelynite; Cpx = pigeonite; Ol = olivine.

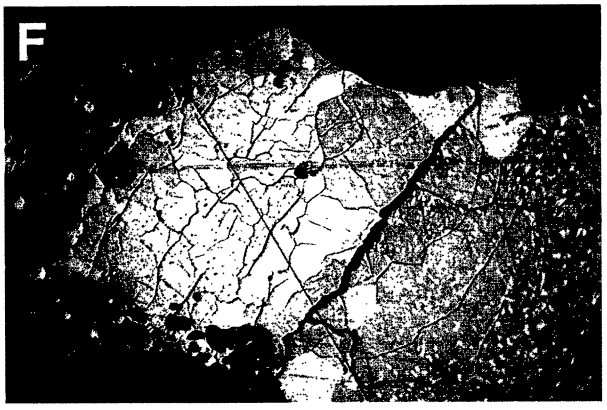

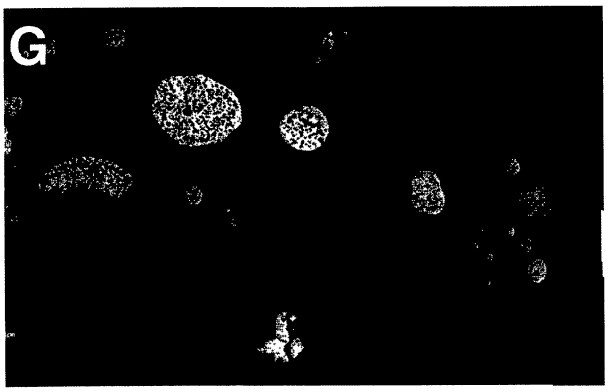

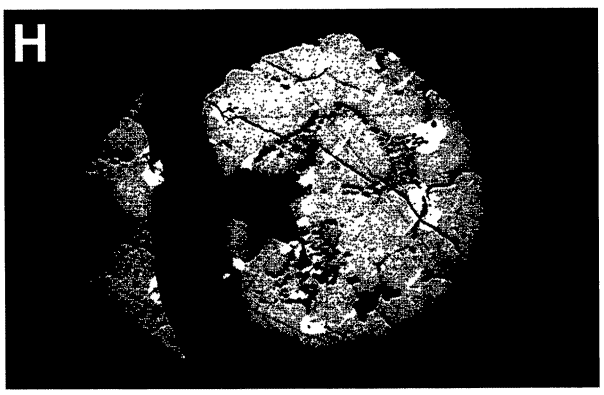

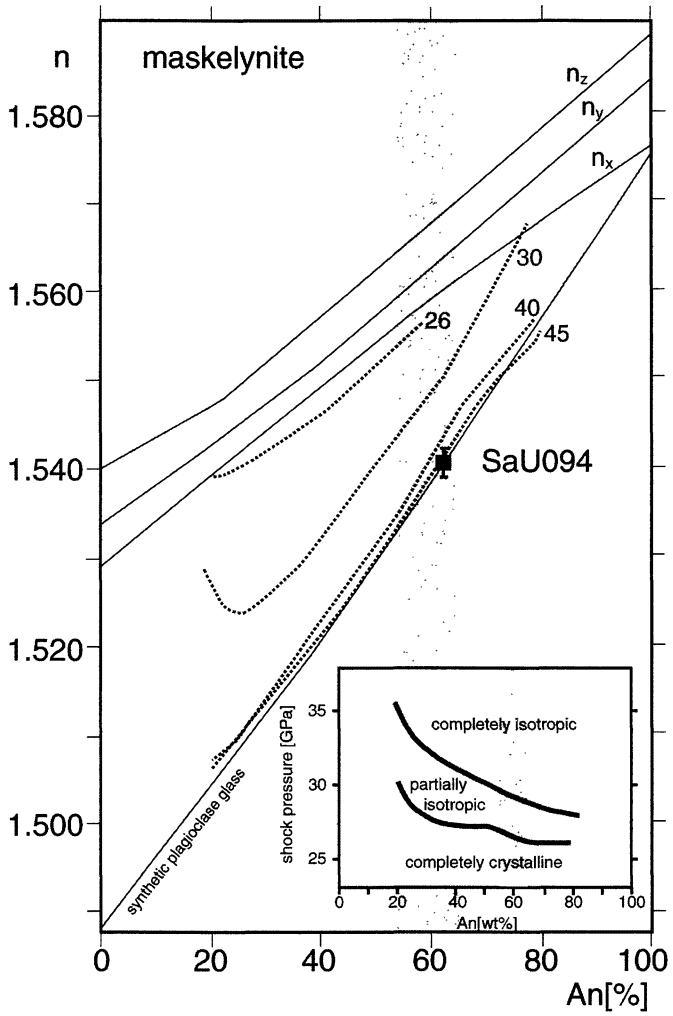

FIG. 10. Minimum shock pressure estimate based on maskelynite chemistry and optical refractive indices. The data indicate shock pressures in excess of 45 GPa throughout the rock. Isobars are from Stöffler (1984).

at room temperatures but no deformation were observed in reflected light, suggesting complete recrystallization. Even the least affected pyrrhotite grains are aggregates of polygonal grains.

Shock-wave and ultra-high pressure experiments on $Fe_{0.9}S$ and FeS compositions were conducted by Brown *et al.* (1984) and Williams and Jeanloz (1990). Their data indicate that shock temperatures of ~3000 K at >45 GPa are needed to melt pyrrhotite. This temperature drops below 2000 K at lower pressures (Fig. 11). Brown *et al.* (1984) noted phase transitions of $Fe_{0.9}S$ with increasing pressure before it melts. This suggests that the equigranular polygonal texture of the pyrrhotite grains in SaU 094 was acquired either during recrystallization after shock deformation (dislocation density too high and post-shock temperature high enough), recrystallization associated with a phase transition, or a combination of the two.

Shock melt pockets form up to 6.7 vol% of the rock. The central parts of larger pockets generally consist of a fresh green glass, locally containing sulfide melt droplets and vesicles (Fig. 3c). The glassy part is separated from the host rock minerals by a dark (macroscopically black) zone of a very fine-grained, polycrystalline silicates (Fig. 3c) also containing globular sulfide droplets and angular oxide fragments. Based on experimental work such melt pockets suggest local shock pressure as high as 80 GPa (*e.g.*, McSween and Stöffler, 1980) accompanied by heating to 1600–2000 °C. The oblate millimeter-sized vesicles are common in glassy and recrystallized shock melts in SaU 094 (Figs. 2 and 3c) and have a preferred orientation (Fig. 4).

Considering all shock features, the shock grade of SaU 094 is S6, according to the scale for chondrites proposed by Stöffler *et al.* (1991). In the original description of SaU 094 (Grossman and Zipfel, 2001) which was based on small fragments lacking melt pockets only S5 was estimated (optically isotropic maskelynite).

OXYGEN ISOTOPES

The oxygen isotopic composition of SaU 094 was initially determined on a 18 mg untreated sample recovered from the surface. Two oxygen isotope measurements on a surface chip yielded $\delta^{17}O$ 2.50/2.51‰, $\delta^{18}O$ 4.30/4.28‰, $\delta^{17}O$ 0.27/0.30‰. The low $\delta^{17}O$ value probably is influenced by the presence of terrestrial calcite. The $\delta^{18}O$ *vs.* $\delta^{17}O$ values plot close to the fractionation line defined by other Mars meteorites (Franchi *et al.*, 1999; Fig. 11). The O isotopic composition of SaU 094 is one of the lightest of the known Mars meteorites, similar to Chassigny.

DISCUSSION

Magmatic History

In comparison with similar shergottites like DaG 476/489/670/735 (*e.g.*, McSween and Treimann, 1998; Zipfel *et al.*, 2000; Folco *et al.*, 2000; Mikouchi *et al.*, 2001) the minerals and glasses in SaU 094 show little zonation (Fig. 6). This implies that the minerals had enough time to chemically reequilibrate during crystallization. Also, the grain size of the groundmass is larger than in typical terrestrial volcanic flows. Both criteria suggest crystallization in a plutonic to subvolcanic environment. Oxygen fugacity conditions were near the Fe/FeO buffer as indicated by the presence of chromite to titanian magnesian chromite and Fe^{3+}-poor ilmenite. Because of the shock oxidation and the weak zoning of olivine megacrysts in SaU 094 no attempts are made here to interpret them as phenocrysts or xenocrysts. However, Zipfel (2000) described the olivines in SaU 005, which we interpret as paired with SaU 094, as phenocrysts, and compared them with DaG 476 where the large olivines were interpreted as xenocrysts (Mikouchi *et al.*, 1999; Zipfel *et al.*, 2000).

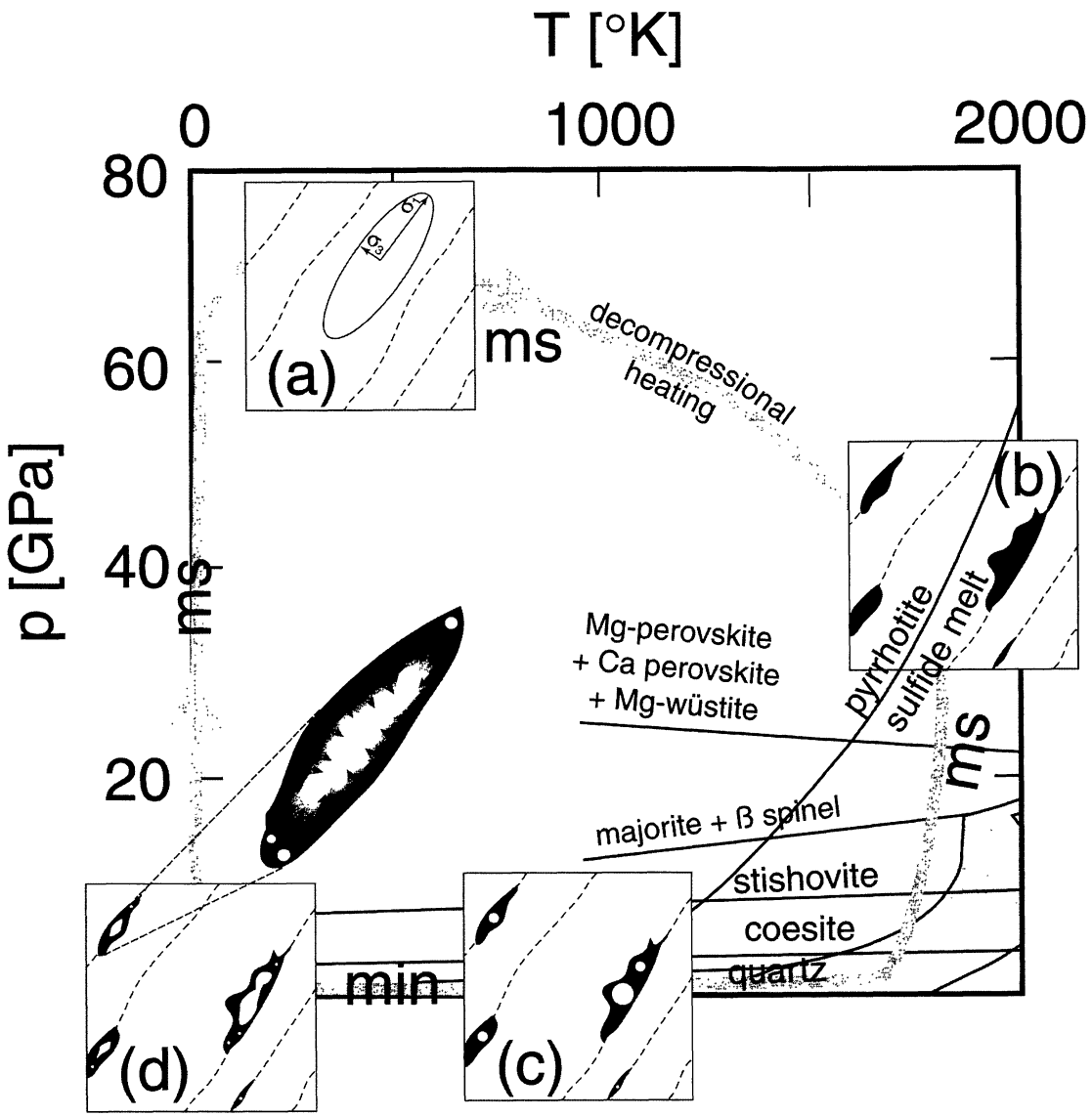

FIG. 11. Schematic diagram showing different steps in the formation of oriented vesicles in melt pockets. Note that not all parts of the rock reached melting conditions. Sulfide melting curve is from Williams and Jeanloz (1990), the SiO_2 polymorph boundaries from Hemley *et al.* (1994), all other phase boundaries from McDonough and Rudnick (1998). ms = milliseconds; min = minutes. For discussion see text.

Considering the trace element distribution, Zn and V are strongly fractionated into chromites, Mn is slightly fractionated into the oxides. Maskelynite concentrates K (and presumably Sr, Ba, Cs, Rb). Co and Ni concentrate in pentlandite and olivine. As, Se, and Cu fractionate mainly into pyrrhotite and pentlandite. REEs are fractionated into merrillite but occur probably also in the other Ca-phases clinopyroxene and plagioclase.

Based on a content of 0.3 wt% sulfides and an average pentlandite volume fraction of 0.085 in the sulfides (derived from image analysis), the NiS fraction in the sulfides averages 7.1 wt%. Using a total Ni of 310 ppm (SaU 005; Dreibus *et al.*, 2000) and KD values for sulfide/silicate partitioning of Ni from the compilation of Naldrett (1989), a range of 3.6–6.6% NiS in the sulfide is predicted. Given the uncertainties, this indicates that the Ni content of the sulfides corresponds to magmatic equilibrium values. The detectable arsenic in the sulfides in SaU 094 indicate that this phase probably is the most important As carrier in the meteorite.

Shock Metamorphism

The shock oxidation of olivines in SaU 094 is similarly strong as that in ALH 77005 (Osterdag *et al.*, 1984) and Lewis

Cliff (LEW) 88516 (Harvey *et al.*, 1993). This suggests a shock-imprint under oxygen fugacity conditions that were relatively high, probably near the martian surface or, alternatively, terrestrial oxidation of shocked olivines. It is evident that during the early stage of shock imprint on Mars some shock-deformed olivines along shock melt pockets melted and recrystallized as clear (Fe^{3+}-poor) olivine.

Interesting is the high amount, large size and the preferred orientation of vesicles in SaU 094, to our knowledge not reported from other shergottites. As the amount of shock melt is similar to other shergottites (*e.g.*, Dar al Gani in Table 1) this may, however, indicate that they have been overlooked. It remains to be confirmed that such oriented vesicles are additional evidence for very high shock pressures (near a fragmentation value).

A model as to how such oriented vesicles may have formed during shock deformation is shown in Fig. 11. An anisotropic shock wave produces oriented deformation bands and fractures in the bulk rock parallel to the main stress direction σ_1 (a). Olivine shock oxidation and crystal plastic, as well as brittle deformation occur during this very early stage. Decompressional heating induces melting in areas of highest dislocation densities (b), and these melt herds propagate along the prestructured rock upon decompression resulting in many cases in elongated melt pockets (b, c). Mineral grain contacts with appropriate minimum melting composition seem not important because melt formation is seen within olivine and pyroxene (see Table 2). The composition of the melt is controlled by the local mineralogy, and only larger pockets reach near bulk-rock composition. Although 2000 K may have been reached at peak pressures (*e.g.*, McSween and Stöffler, 1980), reaching such temperatures by decompression melting is probably more effective, and very likely in our case, where the pyrrhotite melting curve is crossed at lower pressures. During the cooling stage at low pressure silicate melt and fluid (vapor) exsolve to produce globular fluid droplets in a silicate melt (c). As cooling propagates from the walls of melt pockets to the interior, fluid (vapor) migrates and coalesces in the central part of the melt pockets (Fig. 3c). The interplay of diffusion and melt viscosity results in larger, elongated vesicles in the central part of the melt pockets which are recognizable on the tomographs (Fig. 2). Smaller globular droplets remain trapped in the melt pocket glass. We suggest that also the shock melt pockets have a preferred orientation. However, the tomographs do not allow to distinguish shock melt from the rest of the matrix. The elongated shock melt pockets with central, elongated hole are visible in thin section (Fig. 3c). The proposed p–T–t path suggest presence of ultra-high pressure phases like ringwoodite, majorite or $KAlSi_3O_8$ hollandite which were found in similarly strong shocked martian meteorites (Lagenhorst and Poirier, 2000).

Low-Temperature Overprinting

If we assume that shock metamorphism occurred during ejection from Mars, consequently, all oxidation products are of terrestrial origin and SaU 094 shows no obvious signs of pre-terrestrial aqueous alteration. This is also indicated by the absence of pyrite which is present in the majority of martian meteorites. Due to its maximum thermal stability of 743 °C pyrite is an indicator of fluid-driven alteration processes.

Comparison with Dar al Gani 476

Dar al Gani 476/489/670/735/876 and SaU 005/008/051/094 are similar in modal composition, mineralogy, grain size and texture. Direct comparison of SaU 094 and DaG 476 in backscattered images (Fig. 12) indicates that similar zoning in pigeonite is found in both. The chemical variation in DaG 476 is stronger, and even macroscopically visible (Folco *et al.*, 2000; Mikouchi *et al.*, 2001; Wadhwa *et al.*, 2001; Zipfel *et al.*, 2000). Although irregular zoning patterns can occur in magmatic pyroxenes (*e.g.*, by replacement) the zoning is unlike typical magmatic pyroxene growth zoning parallel to the crystal faces (compare Fig. 12b and 12c). The relatively narrow X_{Mg} range of olivine in SaU 094 is similar to lherzolitic shergotties (*e.g.*, McSween and Treimann, 1998) and below the maximum of Fo_{76} found in DaG 476 (Mikouchi *et al.*, 2001). Moreover, SaU 094 shows slight Mg enrichment towards olivine rims (Fig. 6), whereas olivine rims in DaG 476 are Fe-rich. As shock oxidation affects the Fe/Mg ratio of the olivines it is difficult to deduce a magmatic history from the zoning. The anorthite content of the maskelynite is also similar to lherzolitic shergottites and higher than the anorthite content in basaltic shergottites, except DaG. In SaU 005 (Zipfel, 2000; Goodrich and Zipfel, 2001) the observed compositional ranges are $Fo_{63–73}$ (olivine), $En_{70}Wo_6$ to $En_{61}Wo_{13}$ (pigeonite), $En_{47\ and\ 50}Wo_{32}$ (augite) and $An_{51–65}Or_{0.3–0.9}$ (maskelynite). The observed compositional ranges in SaU 094, and the mineral zoning further support that SaU 094 and SaU 005/008 are paired.

A comparison of the magnetic properties of pyrrhotite using the Bitter method (Soffel, 1991) showed that magnetic pyrrhotite in DaG is significantly more abundant, consistent with a stronger magnetization of DaG compared with SaU as reported by Rochette *et al.* (2001). Since rare magnetic pyrrhotite is associated with weathering products in SaU 094, and DaG is more strongly altered, the stronger bulk magnetism of the latter may be related to its degree of terrestrial alteration.

CONCLUSIONS

SaU 094 is a strongly shocked gabbroic shergottitic meteorite with lherzolithic affinities. Its chemistry is very likely that of a basaltic shergottite. Low-temperature alteration products apparently are all of terrestrial origin and there is no obvious pre-terrestrial aqueous alteration. Besides the lower degree of terrestrial weathering, the similarity with DaG 476 and paired shergottites is extremely high.

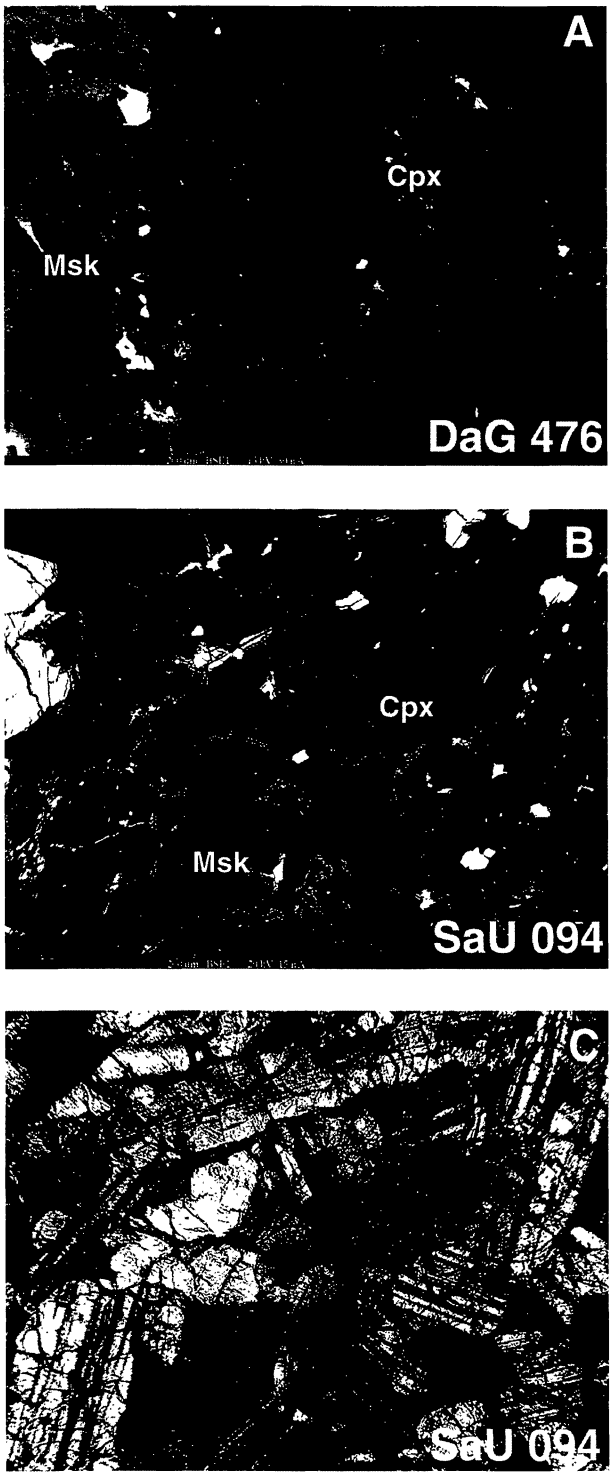

FIG. 12. Comparison of backscattered electron images of pigeonite zoning in DaG 476 (a) and SaU 094, obtained with the same detector. Both samples show similar chemical zoning although the chemical variation is larger in DaG 476. Note that the zoning in SaU 094 in (b) is irregular within a crystal. Grain boundaries are more visible in the optical microscope image (c). The chemical irregularities within one grain are also reflected in the pigeonite single crystal traverses in Fig. 6.

Acknowledgments–A. Flisch (EMPA, Dübendorf), is thanked for operating the x-ray tomograph. Dr. Hilal al Azri, Deputy Director General of Minerals, Ministry of Commerce and Industry is thanked for giving permission for the field work in Oman and logistic support. We thank Tj. Peters for his support during various stages of this project, R. Graf for his help with the photomicrographs, and K. Ramseyer for help on the kathode luminescence machine. Critical reviews by Gordon A. McKay and an anonymous reviewer are greatfully acknowledged.

Editorial handling: H. Nagahara

REFERENCES

BOGARD D. D. AND JOHNSON P. (1983) Martian gases in an Antarctic meteorite. *Science* **221**, 651–654.

BROWN J. M., AHRENS T. J. AND SHAMPINE D. L. (1984) Hugeniot data for pyrrhotite and the Earth's core. *J. Geophys. Res.* **89**, 6041–6048.

CLAYTON R. N. AND MAYEDA T. K. (1996) Oxygen-isotope studies of achondrites. *Geochim. Cosmochim. Acta* **60**, 1999–2017.

CRAIG J. R. AND SCOTT S. D. (1974) Sulfide phase equilibria. In *Sulfide Mineralogy* (ed. P. H. Ribbe), pp. CS-1 to CS-110. Rev. Mineral. **1**, Mineral. Soc. Amer., Washington, D.C., USA.

DOWTY E. (1977) Phosphates in Agra Dos Reis: Structure and composition of the $Ca_3(PO_4)_2$ minerals. *Earth Planet. Sci. Lett.* **35**, 347–351.

DREIBUS G. AND WÄNKE H. (1987) Volatiles on Earth and Mars: A comparison. *Icarus* **60**, 225–240.

DREIBUS G., SPETTEL B., HAUBOLD R., JOCHUM K. P., PALME H., WOLF D. AND ZIPFEL J. (2000) Chemistry of a shergottite: Sayh al Uhaymir 005 (abstract). *Meteorit. Planet. Sci.* **35 (Suppl.)**, A49.

FLEISCHER M., CABRI L. J., CHAO G. Y. AND PABST A. (1978) New mineral names. Ferrifayalite (= laihunite). *Am. Mineral.* **63**, 424–425.

FOLCO L., FRANCHI I. A., D'ORAZIO M., ROCCHI S. AND SCHULTZ L. (2000) A new meteorite from the Sahara: The shergottite Dar al Gani 489. *Meteorit. Planet. Sci.* **35**, 827–839.

FRANCHI I. A., WRIGHT I. P., SEXTON A. S. AND PILLINGER C. T. (1999) The oxygen isotopic composition of Earth and Mars. *Meteorit. Planet. Sci.* **34**, 657–661.

GLEASON J. D., KRING D. A., HILL D. H. AND BOYNTON W. V. (1997) Petrography and bulk chemistry of martian lherzolite LEW 88516. *Geochim. Cosmochim. Acta* **61**, 4007–4014.

GOODRICH C. A. AND ZIPFEL J. (2001) Magmatic inclusions in olivine and chromite in basaltic shergottite Sayh al Uhaymir 005: Implications for petrogenesis and relationship to lherzolitic shergottites (abstract). *Lunar Planet. Sci.* **32**, # 1174, Lunar and Planetary Institute, Houston, Texas, USA (CD-ROM).

GROSSMAN J. N. (2000) The Meteoritical Bulletin, 84. *Meteorit. Planet. Sci.* **35 (Suppl.)**, A199–A225.

GROSSMAN J. N. AND ZIPFEL J. (2001) The Meteoritical Bulletin, 85. *Meteorit. Planet. Sci.* **36 (Suppl.)**, A293–A322.

HARVEY R. P., WADHWA M., MCSWEEN H. Y., JR. AND CROZAZ G. (1993) Petrography, mineral chemistry, and petrogenesis of Antarctic shergottite LEW 88516. *Geochim. Cosmochim. Acta* **57**, 4769–4783.

HEMLEY R. J., PREWIT C. T. AND KINGM K. J. (1994) High-pressure behavior of silica. *Rev. Mineral.* **29**, 41–73.

LAGENHORST F. AND POIRIER J-P. (2000) 'Eclogitic' minerals in a shocked basaltic meteorite. *Earth Planet. Sci. Lett.* **176**, 259–265.

LE MAITRE R. W. *ET AL.* (1989) *A Classification of Igneous Rocks and Glossary of Terms*. Blackwell, Oxford, U.K. 193 pp.

LE MÉTOUR J., MICHEL J. C., BÉCHENNEC F., PLATEL J. P. AND ROGER J. (1995) *Geology and Mineral Wealth of the Sultanate of Oman*. Ministry of Petroleum and Minerals, Directorate General Of Minerals, Sultanate of Oman, Muscat, Oman. 285 pp.

LODDERS K. (1998) A survey of shergottite, nakhlite and chassigny meteorites whole-rock compositions. *Meteorit. Planet. Sci.* **33 (Suppl.)**, A183–A190.

MCDONOUGH W. F. AND RUDNICK R. L. (1998) Mineralogy and composition of the upper mantle. *Rev. Mineral.* **37**, 139–159.

MCKAY D. S., GIBSON E. K. J., THOMAS-KEPRTRA K. L., VALI H., ROMANEK C. S., CLEMENT S. J., CHILLIER X. D. F., MAECHLING C. R. AND ZARE R. N. (1996) Search for past life on Mars: Possible relic biogenic activity in martian meteorite ALH 84001. *Science* **273**, 924–930.

MCSWEEN H. Y. AND JAROSEWICH E., JR. (1983) Petrogenesis of the Elephant Moraine A79001 meteorite: Multiple magma pulses on the shergottite parent body. *Geochim. Cosmochim. Acta* **47**, 1501–1513.

MCSWEEN H. Y. AND TREIMAN A. H. (1998) Martian meteorites. In *Planetary Materials* (ed. J. J. Papike), pp. 6–01 to 6–53. Mineralogical Society of America, Washington, D.C., USA.

MCSWEEN H. Y., JR. AND STÖFFLER D. (1980) Shock metamorphic features in Allan Hills 77005 meteorite (abstract). *Lunar Planet. Sci.* **11**, 717–719.

MIKOUCHI T., MIYAMOTO M. AND MCKAY G. A. (1999) Cooling rates of olivines in the martian meteorites Dar al Gani 476 and Elephant Moraine 79001 (abstract). *Meteorit. Planet. Sci.* **34 (Suppl.)**, A81–A82.

MIKOUCHI T., MIYAMOTO M. AND MCKAY G. A. (2001) Mineralogy and petrology of the Dar al Gani 476 martian meteorite: Implications for its cooling history and relationship to other shergottites. *Meteorit. Planet. Sci.* **36**, 531–548.

MILLER M. F., FRANCHI I. A., SEXTON A. S. AND PILLINGER C. T. (1999) High-precision $\delta^{17}O$ measurements of oxygen from silicates and other oxides: Method and applications. *Rapid Commun. Mass Spectrom.* **13**, 1211–1217.

NALDRETT A. J. (1989) *Magmatic Sulfide Deposits*. Clarendon Press, New York, New York, USA. 186 pp.

MOORE P. B. (1983) Cerite, $Re_9(Fe^{3+},Mg)(SiO_4)_6(SiO_4OH)(OH)_3$: Its crystal structure and relation to whitlockite. *Am. Mineral.* **68**, 996–1003.

OSTERDAG R., AMTHAUER G., RAGER H. AND MCSWEEN, H. Y., JR. (1984) Fe^{3+} in shocked olivine crystals of the ALHA77005 meteorite. *Earth Planet. Sci. Lett.* **67**, 162–166.

PAPIKE J. J. (1998) Comperative planetary mineralogy: Chemistry of melt-derived pyroxene, feldspar, and olivine. In *Planetary Materials* (ed. J. J. Papike), pp. 7–01 to 7–11. Mineralogical Society of America, Washington, D.C., USA.

ROCHETTE P., LORAND J-P., FILLION G. AND AUTTER V. (2001) Pyrrhotite and the remanent magnetization of SNC meteorites; a changing perspective on martian magnetism. *Earth Planet. Sci. Lett.* **190**, 1–12.

SCHERRER N. C., ENGI M., GNOS E., JAKOB V. AND LIECHTI A. (2000) Monazite analysis; from sample preparation to microprobe age dating and REE quantification. *Schweiz. Mineral. Petr. Mitt.* **80**, 93–105.

SOFFEL H. C. (1991) *Paläomagnetismus und Archäomagnetismus*. Springer, Berlin, Germany. 276 pp.

STEELE I. M. AND SMITH J. V. (1982) Petrography and mineralogy of two basalts and olivine-pyroxene-spinel fragments in achondrite EETA97001. *J. Geophys. Res.* **87**, A375–A384.

STÖFFLER D. (1984) Glasses formed by hypervelocity impact. *J. Non-Cryst. Solids* **67**, 465–502.

STÖFFLER D., KEIL K. AND SCOTT E. R. D. (1991) Shock metamorphism of ordinary chondrites. *Geochim. Cosmochim. Acta* **55**, 2845–3867.

STRECKEISEN A. (1976) To each plutonic rock its proper name. *Earth Sci. Rev.* **12**, 1–33.

TREIMAN A. H. (1990) Complex petrogenesis of the Nakhla (SNC) meteorite: Evidence from petrography and mineral chemistry. *Proc. Lunar Planet. Sci. Conf.* **20th**, 273–280.

TREIMAN A. H., MCKAY G. A., BOGARD D. D., MITTLEFEHLDT D. W., WANG M-S., KELLER L., LIPSCHUTZ M. E., LINDSTROM M. M. AND GARRISON D. (1994) Comparison of the LEW 88516 and ALHA77005 martian meteorites: Similar but distinct. *Meteoritics* **29**, 581–592.

WADHWA M., LENTZ, R. C. F., MCSWEEN H. Y., JR. AND CROZAZ G. (2001) A petrologic trace element study of Dar al Gani 476 and Dar al Gani 489: Twin meteorites with affinities to basaltic and lherzolitic shergottites. *Meteorit. Planet. Sci.* **36**, 195–208.

WÄNKE H. (1991) Chemistry, accretion and evolution of Mars. *Space Sci. Rev.* **56**, 1–8.

WILLIAMS Q. AND JEANLOZ R. (1990) Melting relations in the iron-sulfur system at ultra-high pressures: Implications for the thermal state of the Earth. *J. Geophys. Res.* **95**, 19 299–19 310.

ZIPFEL J. (2000) Sayh al Uhaymir 005/008 and its relationship to Dar al Gani 476/489 (abstract). *Meteorit. Planet. Sci.* **35 (Suppl.)**, A178.

ZIPFEL J., SCHERER P., SPETTEL B., DREIBUS G. AND SCHULTZ L. (2000) Petrology and chemistry of the new shergottite Dar al Gani 476. *Meteorit. Planet. Sci.* **35**, 95–106.